

# Buckling and interface strength analyses of thermal barrier coatings combining Laser Shock Adhesion Test to thermal cycling

Vincent Guipont, Geoffrey Bégué, Grégory Fabre, Vincent Maurel

▶ **To cite this version:**

Vincent Guipont, Geoffrey Bégué, Grégory Fabre, Vincent Maurel. Buckling and interface strength analyses of thermal barrier coatings combining Laser Shock Adhesion Test to thermal cycling. Surface and Coatings Technology, 2019, pp.124938. 10.1016/j.surfcoat.2019.124938 . hal-02308106

**HAL Id: hal-02308106**

**https://minesparis-psl.hal.science/hal-02308106**

Submitted on 21 Jul 2022

**HAL** is a multi-disciplinary open access archive for the deposit and dissemination of scientific research documents, whether they are published or not. The documents may come from teaching and research institutions in France or abroad, or from public or private research centers.

L'archive ouverte pluridisciplinaire **HAL**, est destinée au dépôt et à la diffusion de documents scientifiques de niveau recherche, publiés ou non, émanant des établissements d'enseignement et de recherche français ou étrangers, des laboratoires publics ou privés.



Distributed under a Creative Commons Attribution - NonCommercial 4.0 International License

Version of Record: https://www.sciencedirect.com/science/article/pii/S0257897219309193
Manuscript_50b2c0194cc57828c762d5149f2b54c4

# Buckling and Interface Strength Analyses of Thermal Barrier Coatings combining Laser Shock Adhesion Test to Thermal Cycling

Vincent Guipont[a], Geoffrey Begue[a], Gregory Fabre[a], Vincent Maurel[a,*]

[a] *MINES ParisTech, PSL Research University, MAT - Centre des Materiaux, CNRS UMR 7633, BP87, 91003 Evry, France*

**Abstract**

Laser Shock Adhesion Test (LASAT) is a non-contacting technique that can be applied to evaluate the interfacial adherence of ceramic layer on metallic substrate. This study aims at combining the laser-induced delamination and blistering when applied to a conventional EB-PVD TBC submitted to thermal cycling. Besides, the use of white spot diagnostic as a NDT technique and 3D profilometer measurement along thermal cycling were fully consistent. The LASAT analysis of as-deposited samples with various initial substrate roughness is discussed regarding the corresponding life to top-coat spallation under air thermal cycling. Mixing thermal cycling with LASAT has enabled to show that the adherence was sensitive to process condition consistently with the performance measured by conventional thermal cycling tests. Moreover, the evolution of the adherence has also been be assessed by LASAT applied to TBC samples with different interrupted thermal cycling conditions. According to this methodology, LASAT could also be used to introduce an interfacial defect known in location, size of debonded area, height of the blister and number of cycles. After further interrupted thermal cycling, the crack propagation and the buckling were monitored. Such measurements allowed to derive the interfacial toughness corresponding to these various aging conditions.

*Keywords:* thermal barrier coating, interfacial toughness, buckling, laser shock, LASAT, thermal cycling, EB-PVD

## 1. Introduction

Thermal barrier coatings (TBCs) are porous ceramic deposited on parts to protect components in hot sections of gas-turbine aero-engines [1]. Electron Beam - Physical Vapour Deposition (EB-PVD) TBCs exhibit typical columnar microstructure. This microstructure is recommended for parts having the most severe service conditions like high pressure rotating blades and stationary vanes in jet engines. Thus, when ceramic coating spalls off, it results in a loss of the insulating properties that can be highly detrimental for the service life of the part. Industrially, the lifetime of TBCs is assessed on free-standing coated buttons by implementing thermal cycling tests to measure the number of cycles before the occurrence of a 20% spalled surface [2]. To mimic more closely service loading, fatigue tests combining the cycling of both thermal and mechanical loads can be achieved [3]. Such advanced analysis is necessary to build relevant damage based life model for TBC [4].

With thermal aging, interfacial micro-cracking, interfacial delamination of the ceramic top-coat (TC) and further buckling, cracking and spallation of the ceramic top-coat will append [2, 5]. Experimentally, a thermal cycling test ends when the spallation is obviously generalized and fully visible. This is an actual limitation of such test because the early stage of the damaging process could not be addressed pushing the need of methodology of interface damage analysis limiting associated artifact. The examination of cross-sections combined with interrupted cycles to measure the evolution of the interfacial damage can be

*Corresponding author
*Email address:* vincent.maurel@mines-paristech.fr (Vincent Maurel)



© 2019 published by Elsevier. This manuscript is made available under the CC BY NC user license
https://creativecommons.org/licenses/by-nc/4.0/

envisaged but this approach is destructive and requires a series of specimen [6]. For interrupted aging (i.e. before spontaneous spallation of the TC), compressive testing up to TC spallation can be used to derive damage evolution from inverse analysis [4, 7]. A non-destructive method to monitor the residual stress within the TGO throughout the ceramic TC by piezo-spectroscopy can be correlated to the mapping of the damage during aging [6, 8]. Recent progress in X-ray computed tomography and laminography have also enabled to assess the local delamination using synchrotron source of energy but the image resolution are still rather low while the size and number of scanned samples are limited by the complexity of the technique [9, 10]. To increase the spatial resolution, the association of focused ion beam coupled with scanning electron microscopy (FIB-SEM) 3D serial sectioning tomography was seen to be fully relevant for EB-PVD TBC, where details of interface microstructure morphology are obtained with a resolution of tens of nm [11]. But again, the time cost of preparation and time for 3D analysis both limit this technique to very few samples. Alternatively, in case of EB-PVD TBC and other ceramic deposits by plasma spray with thickness ranging up to 200-250 $\mu$m, it has been found that an interfacial crack can be easily detected by optical imaging in the visible spectrum [12, 13]. Infrared thermography imaging can also be used for such non-destructive damage analysis [14]. Indeed, the presence of an interfacial crack affects both the optical and thermal conductivity properties of the deposit in contact with a metal due to the presence of an air gap in-between [12, 13, 14, 15]. If the contrast and the resolution of the rendering image (optical or infrared) is high enough, a direct analysis of the damaged area can be implemented with further measurement using conventional image analysis. This approach for a non-destructive diagnostic of the debonding has been extensively investigated through the development of the Laser Shock Adhesion Test (LASAT) applied to ceramic coatings using so-called "white spot" diagnostic. From thorough comparisons of different non-destructive imaging methods with cross-sections views on various ceramic coatings, it was established that actual cracked areas and corresponding objects observed on top-surface have similar dimensions [13, 16].

The measurement of interface strength using a laser shockwave spallation technique with nanosecond laser source has been investigated since 1990 on various thin films and thick coatings [17, 18, 19, 20]. Based on this premise, the LASAT was developed as bonding test for thick coatings [12, 21, 22]. A first alternative protocol of the conventional LASAT has been introduced on hydroxyapatite ceramic coatings [12]. With such ceramic, the debonding threshold, measured in GW/cm$^2$ and calculated in MPa, was determined by a simple diagnostic with the visual inspection of the ceramic top surface. From such approach, a new concept to control adhesion was developed recently on various ceramic coatings by plotting the crack diameter as a function of the laser power density [22, 13, 23]. The resulting plots, the so-called LASAT-2D curves, systematically revealed that the size of the debonded area increased with the laser energy. This phenomenon can be explained by the role of edge effects on shockwave propagation and their influence on the stress profile at the interface. Indeed, two-dimensional (2D) effects are initiated when the released shockwave propagates spherically from the edge of the irradiated spot. When the laser spot diameter is large enough as compared to the target thickness, 2D effects can be neglected and a top-hat distribution may be assumed. With other geometries, actual 2D effects will contribute to move to a Gaussian-like distribution at the interface [24, 22]. Therefore, for laser energies above the debonding threshold, the size of the crack varies with laser energy. Qualitatively, two similar ceramic coatings having same dimensions but different adhesion levels will be easily discriminated according to the size of the cracked area for each tested laser energy. This effect leads to a variation of the relative position on the ordinate axis of their LASAT-2D curves. Thus, LASAT-2D curves are reproducible and easy to achieve for comparative studies of adhesion. Derived from LASAT experiments, a quantitative approach has been further developed in order to investigate the crack behaviour of blisters prepared by laser shock and further submitted to quasi-static loading [14]. Experimentally, the out-of-plane displacement and the crack growth rate of a plasma-sprayed alumina coating were recorded in situ. The Finite Element Analysis (FEA) modelling of the blister evolution involving Linear Elastic Fracture Mechanics (LEFM) and Cohesive Zone Model (CZM) showed the main influence of failure mode II combined to mode I that resulted in a diamond-like shape for the blister under macroscopic in plane shear loading [14]. Thus LASAT appears as an excellent candidate for building strategy of characterization of aging including the assessment of both the reliability of the method and the interfacial toughness associated to a given defect processed by LASAT.

In the present work, two complementary approaches are proposed by combining the LASAT with thermal

cycling applied to conventional EB-PVD TBCs. First, the evolution of the interface strength measured by LASAT is adressed in the as-received and after thermal cycling for different types of bond-coat (BC) finish. To get into more details, interrupted thermal cycles was used to clarify the progressive impact of aging, using both LASAT and cross-sections examinations. The second approach corresponds to the experimental analysis of the buckling behaviour of one blister initially generated by laser shock and further submitted to interrupted thermal cycles. From a series of 3D profiles recorded on the same blister after different numbers of cycles, an analytical calculation of the TBC interface toughness and its evolution with thermal cycling is proposed.

## 2. Materials and methods

### *2.1. EB-PVD TBC samples*

Industrial TBCs were produced on Ni-based single crystal AM1 superalloy with (Ni,Pt)Al bond-coat (BC) and EB-PVD $ZrO_2$-7%$Y_2O_3$ top-coat (TC), see e.g. [25] for bond-coat and substrate microstructure details. Disks (25 mm in diameter and 2 mm in thickness) and rectangular plates (50 × 30 × 2 $mm^3$) samples were prepared with a 180 $\mu$m thick top-coat. In case of disk specimens, three different bond-coat roughness levels were achieved prior to processing the EB-PVD coating. A reference substrate roughness was obtained by a conventional alumina grit-blasting (GB), referred to as reference case, a high roughness level was achieved by grit blasting with higher propelling gas pressure in the nozzle, referred to as heavy GB and a polished bond-coat sample was also prepared (grit paper SiC P600) to have a low roughness level, referred to as polished case in the sequel.

### *2.2. LASAT experiments*

#### *2.2.1. LASAT facility and laser shock configurations*

LASAT experiments were achieved with a Nd-YAG laser source (SAGA 330, THALES LASER, France) producing a Gaussian 5.2 nm pulse with a 532 nm radiation wavelength having a 2 joules maximum energy. The laser shock diameter is adjusted by a converging lens to apply laser power density from 0.1 GW/$cm^2$ to 10.0 GW/$cm^2$ with laser diameters ranging from 1 to 4 mm typically. In case of EB-PVD TBCs, two different laser shock configurations can be applied by implementing the irradiation on the metallic side (MS mode) or on the ceramic side (CS mode). For the conventional MS mode, the laser interacts directly with the metal with water as confining medium. In case of the CS mode, an adhesive vinyl black tape is used as ablative layer and a transparent adhesive tape as confining medium is preferred [13].

#### *2.2.2. LASAT protocol*

Qualitative assessments of adhesion levels were determined through the analysis of LASAT-2D curves using the "white spot" diagnostic. According to this protocol, the total number of shocks depends on the surface available, the laser shock diameter and the size range of the resulting debonded area. For the latter, due to the potential variation of adhesion between samples, this range might be different. Therefore, due to the easiness of the "white spot" diagnostic, the selection of laser energy is done gradually in order to maximize the number of laser shocks leading to debonded zones. In this work, a 3 mm laser diameter was selected for the whole specimen series. Complementary LASAT experiments were also achieved using 2 and 4 mm in order to investigate the origin of the buckling induced by laser shock.

### *2.3. Observations and analyses*

The ceramic surface optical images were digitized using a high-resolution flatbed image scanner (EXPRESSION 1640XL, EPSON, France) with enhanced contrast settings. The contour of white spot was fitted manually by a circle to access to the measurement of its diameter. 3D profiles of blisters were recorded by optical profilometry (Altisurf 500, Altimet, France). The roughness profile was removed by a Gaussian filter (cut-off length: 0.8 mm). From the resulting surface profile, a 2D profile of the blister is extracted along one of its diameters. This 2D profiles yields the blister maximum height and the shape of the region at the bottom of the blister where the ceramic coating starts to debond from the substrate. Observations of resin

mounted and polished cross-sections were achieved by scanning electron microscope (SEM) (LEO1450VP, LEO Electron Microscopy Ltd, England) with back-scattered electrons detector.

### *2.4. Thermal cycling*

Thermal cycling with 1 hour cycle at 1100 °C was achieved in air furnace with the following time-temperature settings: heating step up to 1100 °C during 10 min., dwell at 1100 °C during 50 min., cooling step during 15 min maximum to reach 100 °C before next cycle, the cooling step being assisted by air jet flow.

### *2.5. Influence of surface preparation and evolution of the interface strength with thermal cycling*

In case of disk-shaped coupons, the interface strength was investigated for each bond-coat roughness processing condition (high/conventional medium/low roughness associated respectively to heavy GB, reference and polished cases) in the as-deposited condition and after 200 cycles of 1 hour at 1100 °C in air using different samples. Each sample was shocked with increasing laser energy to establish the LASAT-2D curves as a function of both initial bond-coat roughness (high/conventional medium/low) and aging. Cross-sectioning has been achieved before and after thermal cycling using diamond cut saw and polishing down to grad 1200 SiC paper.

### *2.6. Evolution of the interface strength during thermal cycling*

Further investigation of the evolution of the interface strength during thermal cycling was investigated by LASAT in the case of rectangular plate sample having the reference roughness. The intent was to follow the evolution of the LASAT 2D curves established at 0 (as received) and up to a maximum of 500 cycles on the same sample submitted to interrupted thermal cycles. To that purpose, the number of laser shocks needed to establish the LASAT-2D curve were adjusted after each interruption. This experimental procedure was decided to allow a representative monitoring of the actual evolution of the system tested by LASAT on the same sample before its full spallation.

## 3. Results of adhesion assessed by LASAT

### *3.1. TBC microstructure and adherence for different processing conditions in the as-processed and after thermal cycling*

Cross-sections in the as-received condition have been observed in back-scattering electrons (BSE) mode to distinguish BC, TGO and TC, Figure 1. For all cases, the interfaces between TC and TGO and between TGO and BC do not present initial debonding. Few interfacial defects have been indicated by black arrows on magnified images, but are seldom observed. Besides, the columnar structure of the TC is directly function of local roughness: the higher the local roughness the higher corn-like defects at the bottom of the columns, compare magnified regions of Fig. 1(a) and Fig. 1(b). Oxide thickness ranges from 700 nm to 1 $\mu$m, for the three-tested configurations. After 200 cycles, the initial roughness impacts directly the roughness evolution and the interfacial debonding, Figure 2. For the reference grit-blasting (GB), few sites of debonding have appeared together with an amplification of both the oxide thickness and roughness of the global TC/BC interface; see black arrows in Fig 2(a). The so-called rumpling effect impacts directly the local roughness with oxide thickening. For heavy GB, this effect is more pronounced and has led to a higher density of debonded sites and larger crack opening, see black arrows in Fig 2(b) and compare magnified regions in Fig 2(a) and Fig 2(b), the rumpling being higher when associated to initial defect and/or local delamination. On the other hand, for polished sample, the roughness after thermal cycling is less pronounced that for other samples and no obvious debonding has been observed. Moreover, the slight increase in roughness seems in this case being limited to modification of the only BC/TGO interface, Fig. 2(c). Oxide thickness ranges from 2 to 4 $\mu$m, for the three-tested configurations. To determine the impact of surface processing conditions, thermal cycling has been conducted up to ceramic spallation (20% minimum), see Table 1. The life to spallation has been increased for both heavy grit blasted and polished surface preparations as compared to conventional grit blasting. Thus, while more interfacial defects have been observed for heavy grit blasting, a less rough

interface associated to a lower content of interfacial defects observed for the reference case did not increase the life to TC spallation. However, for a smooth interface exhibiting a smooth and coherent interface in the as-deposited state like for the polished condition, it was obvious that the resistance to spallation was drastically improved because the thermal cycling was interrupted without any observation of TC damage.

Table 1: Number of cycles to TC spallation; mean and standard deviation (std) values for different surface processing; (*) for polished condition the thermal cycling was interrupted without observation of TC spallation

| | Reference GB | Heavy GB | Polished |
|---|---|---|---|
| Mean | 1097 | 1484 | >1648 |
| Std | 176 | 131 | (*) |

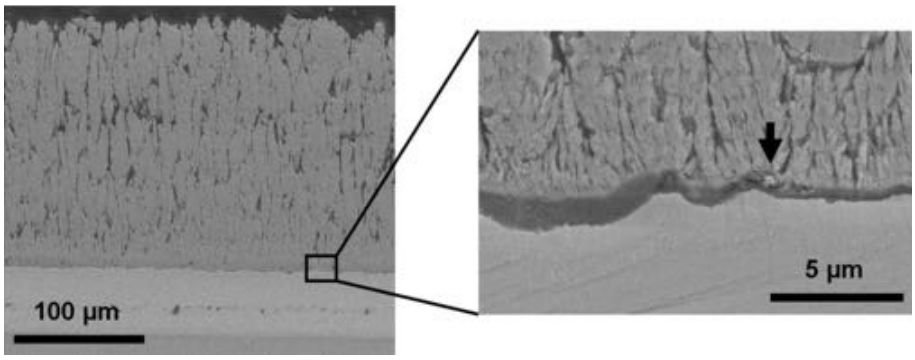
Using LASAT with increasing laser energy combined to white spot diagnostic, the LASAT-2D curves have been established for the whole set of conditions tested: reference, heavy grit blasting and polished surface in the as-received condition and after 200 thermal cycles, Figure 3. For reference processing condition, the LASAT-2D curve obtained after 200 cycles is above the one obtained for the as-processed condition, Fig 3(a). That is to say that for any laser energy, the diameter of the debonded area is higher after aging than for the same LASAT condition tested for as-processed sample. The LASAT-2D curve after 200 cycles exhibits some large variations in debonded area for laser flux above 3 GW/cm$^2$. However, using a log function to fit the experimental results (see continuous lines in Fig. 3) enables to observe a clear ranking for each tested condition. For heavy grit blasting, the same effect is observed: thermal cycling decreases the adherence of the TC, Fig 3(b), but with a lower variation in debonded areas for the whole set of laser flux. As a side note, the as-received condition seems to be more adhesive for high grit blasting as compared to the reference case. However, after 200 cycles, the LASAT-2D curves are very similar for these two conditions. On the other hand the polished samples exhibit a much lower debonding, leading to lower debonding after 200 cycles than observed for the as-processed condition, Fig. 3(c). As a major result, it appears that the final life to spallation is fully consistent with these observations: the polished samples exhibit both the longest life to spallation and the lowest 2D-LASAT curve after 200 cycles. Such demonstration of consistency was obtained using a few number of specimens. Nevertheless, it opens for further thorough study in order to better establish the actual influence of the process condition on the life of coated component using LASAT as a guiding tool to improve the strength of interfaces.

Because this set of LASAT tests was achieved on relatively small disks, we have preferred to establish only LASAT-2D curves without any cross-sectioning before laser shock. Thus full analysis of LASAT and associated cross-sectioning on larger specimen are detailed in the next section.

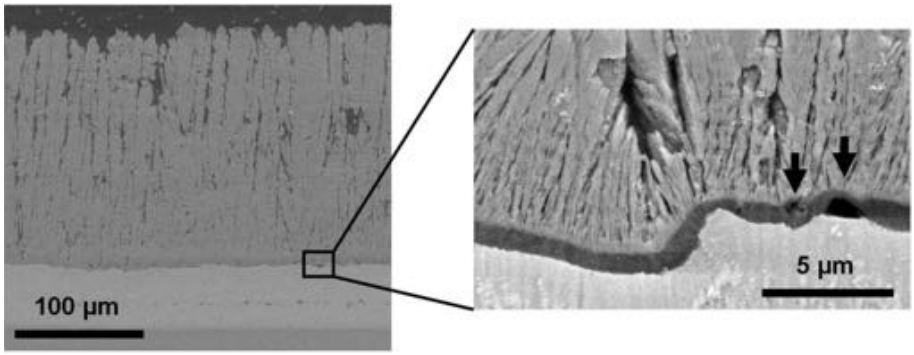
### *3.2. Evolution of adherence with thermal cycling for conventional process*

We established above that LASAT-2D curves evolve consistently with processing parameters (here focused on roughness), aging and interfacial damage observation. This part is now devoted to a single process condition, the above reference GB processing condition, detailed for a larger specimen. The specimen is the rectangular plate of (50 × 30 × 2) mm$^3$ where laser shock series have been achieved for as-processed condition, 10, 50, 100, 250 and 500 cycles. For this specimen, laser shock series led to buckled areas without any spallation of the top-coat induced by the shockwave but also by the thermal cycling during 500 cycles, Figure 4(a). The LASAT-2D curves have been fited with a logarithmic assumption from 1 to almost 3 GW/cm2, Fig. 4(b). Experimentally, the buckled areas were obviously larger when the number of cycles increased. Therefore, the number of laser conditions had to be drastically reduced with only two conditions in case of 250 and 500 cycles.

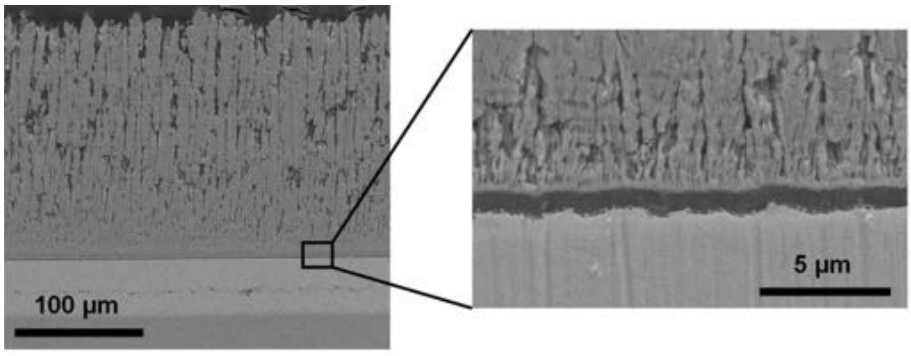
In the as-processed condition, the obtained LASAT-2D curve exhibits the smallest debonded area for a 1.4 GW/cm$^2$ shock, Fig. 4(b). After 10 cycles, the observed debonded area diameters are smaller than in the as-processed condition for the same applied laser power density, appearing as a reinforcement of the




(a) Reference




(b) Heavy GB




(c) Polished

Figure 1: SEM-BSE observation in the as-processed condition for (a) reference, (b) heavy grit-blasting and (c) polishing before BC deposition

interface adhesion. For 50 to 500 thermal cycles, the measured debonded area diameters increase with the number of cycles. This effect is evidenced when plotting the debonded diameter for a 1.6 GW/cm$^2$ shock as a function of the number of cycles, using experimental value or interpolated ones if no value was available for the considered energy, Fig. 4(c). Besides, the smallest debonded area diameters are much larger than

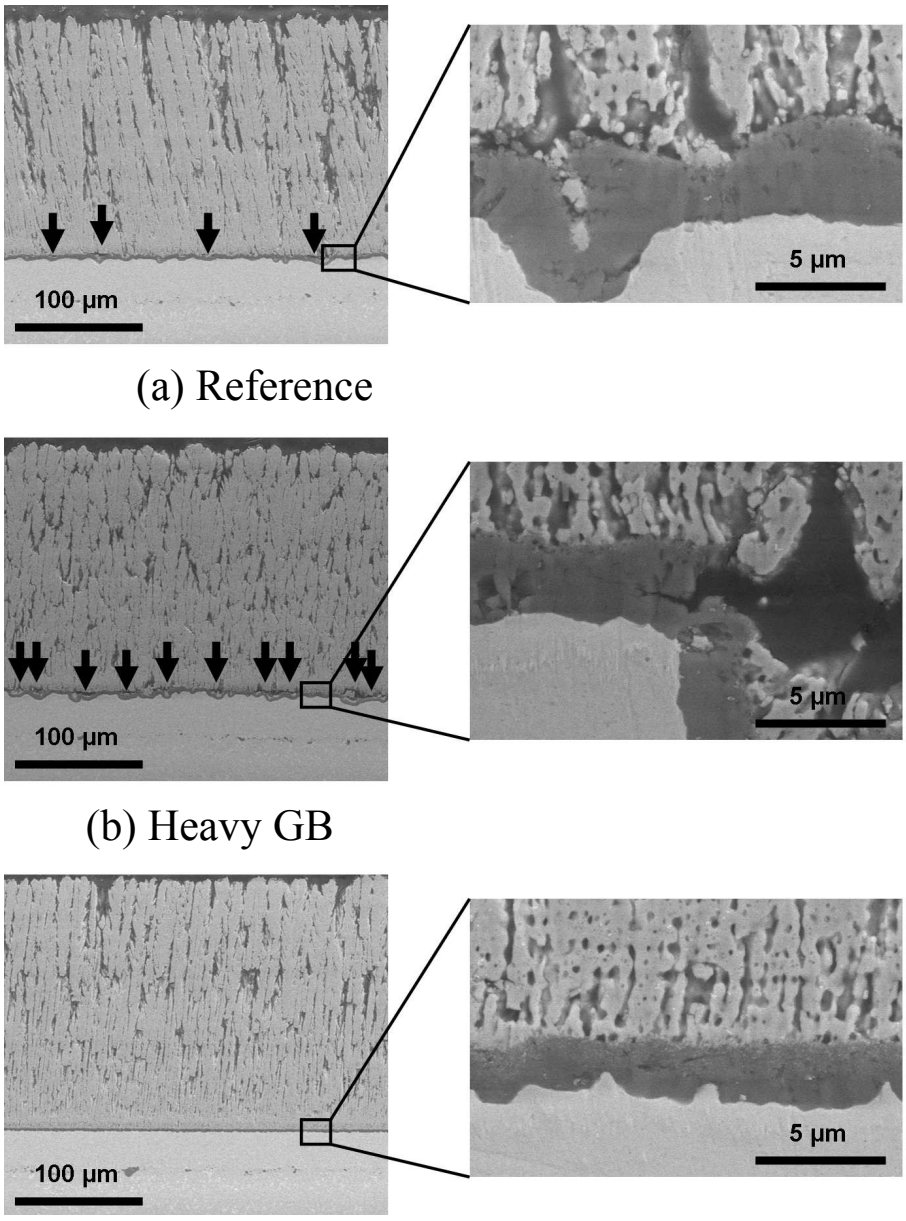
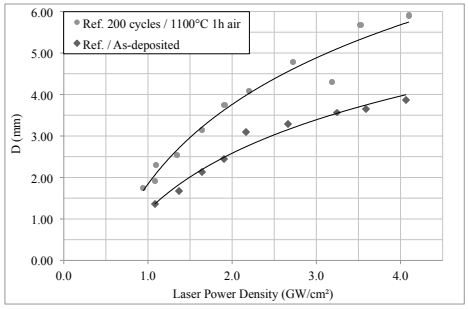


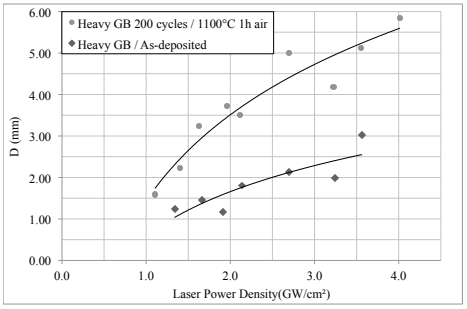

Figure 2: SEM-BSE observation after 200 thermal cycles at 1100 °C/1h for (a) reference, (b) heavy grit-blasting and (c) polishing before BC deposition

the one measured in the as-processed condition, for the lowest applied laser power density. Aging acts both on the size of the debonded area for a given laser power density and on the value of the so-called LASAT threshold, that is to say the minimum laser power density yielding TC debonding.

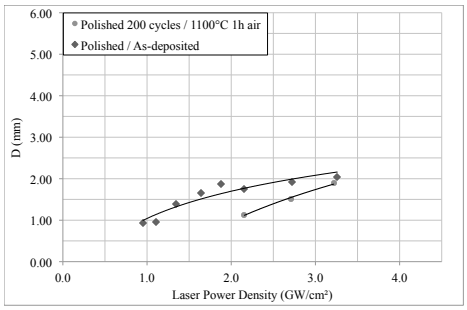
To establish interfacial behaviour by LASAT and cross sectioning, another rectangular sample of (50 × 30 × 2) $mm^3$ has been cut into 6 pieces of (15 × 12 × 2) $mm^3$. Again, the reference GB processing condition has been used. Thus, for the same aging conditions, namely as-received condition, 10, 50, 100,




(a) Reference




(b) Heavy GB




(c) Polished

Figure 3: LASAT-2D curves in the as-processed and after 200 thermal cycles at 1100 °C/1h for (a) reference grit-blasting, (b) heavy grit-blasting and (c) polishing before BC deposition

250 and 500 cycles, only a single laser shock has been applied at a laser power density of 1.6 GW/cm$^2$. For all tested conditions, white spot was observed and cross-section was achieved through one diameter of the white spot by progressive polishing up to reach a maximum value of apparent diameter, Fig. 5(b). In the as-received condition, laser shock has induced partial failure within the TC layer, mainly at the bottom of the columns and parallel to the interface. After only 10 thermal cycles, the crack induced by the laser shock is located at the TC/TGO interface. This localization of crack is observed for all the other aging conditions. However, some partial TC failure are observed but are more or less limited to areas where locally some columnar defects or intrusion of oxide in the BC are observed. Thus, induced LASAT cracks are mostly located at the TC/TGO interface which interface is known to be the weak interface for EB-PVD/(Ni,Pt)Al TBCs after thermal cycling. SEM analyses for the same specimen, but in areas away from laser shock have been also achieved for comparison purpose, Fig. 5(a). For the as-received condition, the location of the crack is consistent with the location of defects at the bottom of the TC, compare Figs. 5(a) and 5(b) at 0 cycle. For any aging condition, the observed oxide thicknesses and local undulation, associated to the so-called rumpling phenomenon, are consistent for both series of observation. After 10 cycles, micro-cracks are evidenced at the TGO/TC interface away from LASAT, and in shocked area: LASAT induced cracks are also localized at the same interface. Thus, the observed apparent reinforcement after 10 cycles is due to a clear modification of damage mechanism induced by aging and a subsequent modification of laser shock induced delamination. It appears that the weakest interface becomes the TGO/TC interface as soon as some micro-cracking has started.

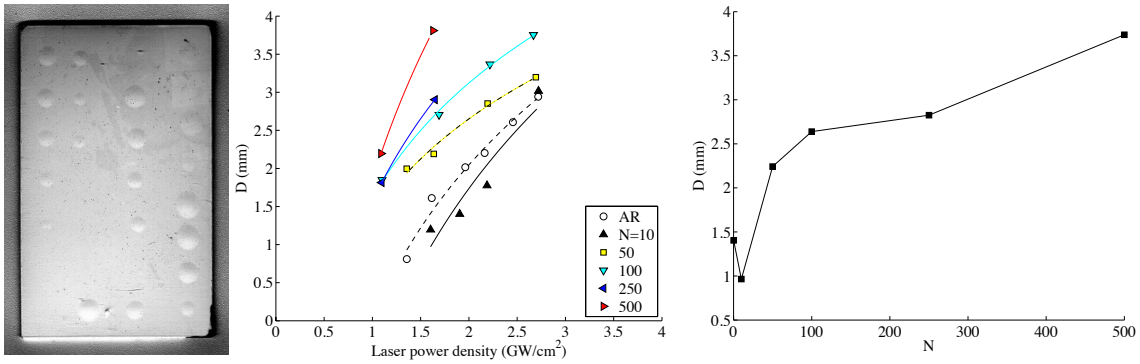


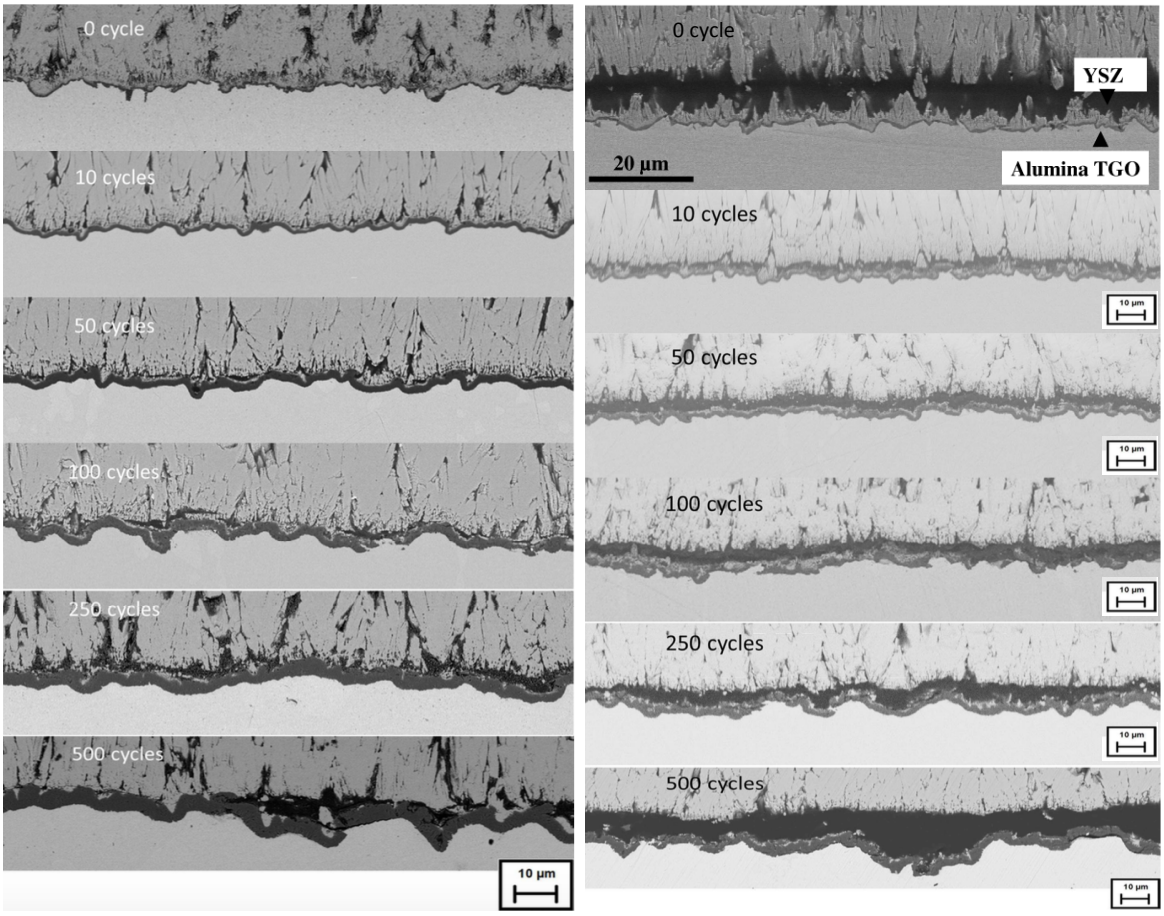

Figure 4: LASAT applied to reference process condition on a rectangular sample (a) surface observation after 500 cycles and (b) LASAT-2D curves for as-processed to 500 thermal cycles at 1100 °C/1h (c) evolution of debonded diameter as a function of the number of thermal cycles for a laser power density of 1.6 GW/cm$^2$.

## 4. Evolution of blistering with thermal cycling

The above results raised two questions 1) does LASAT conditions (laser power density and shock diameter) impact the blistering of the ceramic layer? 2) how evolves a given debonded area introduced by LASAT with further thermal cycling? To handle with these two points, complementary experiments have been achieved using a surface topography mapping together with debonded area measurement with white spot analysis.

### *4.1. Buckling and debonding*

Another series of LASAT-2D curves have been established on a rectangular sample of (50 × 30 × 2) mm$^3$ obtained in the reference processing condition. In this experiment, the LASAT was achieved using 2, 3 or 4 mm for the laser shock diameter after 200 thermal cycles. The results are summarized in Fig. 6(a). It




(a) (b)

Figure 5: SEM-BSE observation of cross-section for as-processed to 500 thermal cycles at 1100 °C/1h (a) away from the laser shock location (b) through the blister induced by laser shock

showed that a change in laser diameter modified the LASAT threshold and also the relative position of the LASAT-2D curve. The higher is the laser shock diameter, the higher is the position of the LASAT-2D curve and the lower is the debonding threshold. These results are fully consistent with calculations of the shockwave propagation that led to different spatial distribution and levels of stress when changing the laser diameter for a sample having the same failure threshold [26]. Using profilometry, the whole surface profile of the different blisters can be obtained yielding the maximum blister height for any tested conditions in function of its diameter measured with the white sport analysis, Fig. 6(b). This observation results in a blister that appeared for a debonded area diameter between 1.6 and 2 mm. For higher debonded area diameters, the blister amplitude was obviously increased (without external damaging) to reach 30 $\mu$m in height for a debonded diameter of about 4 mm. According to this LASAT experiment, it is worth to note that the various shockwave distribution induced by various laser shock diameter did not affect the resulting buckling behaviour of the TBC sample. Therefore, it is claimed that the buckling phenomenon is not affected by the laser shock condition but generated by the sudden crack induced at the interface and further driven by the release of the (compressive) residual stress initially present in the TC and induced by the processing conditions.

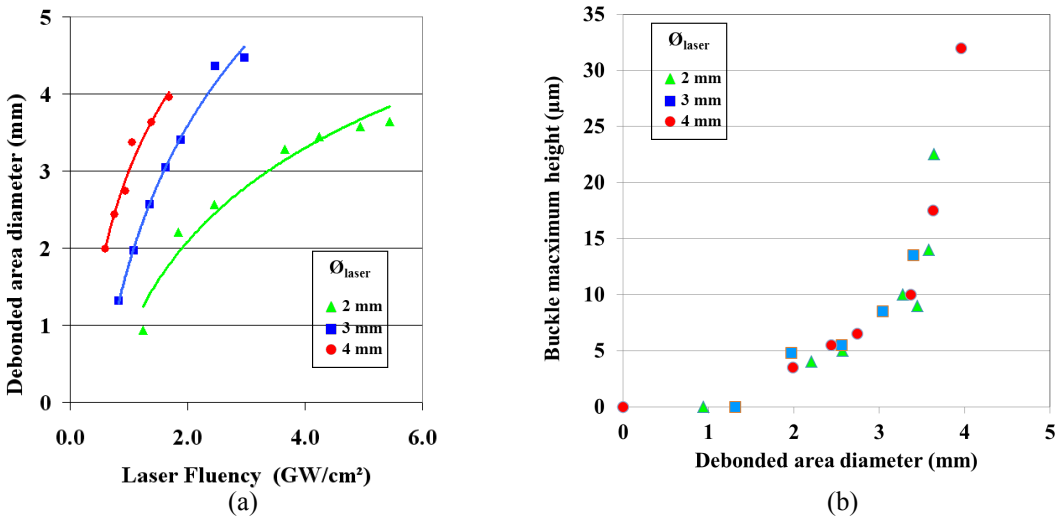



Figure 6: LASAT applied to reference process condition on a rectangular sample (a) LASAT-2D curves for 2mm (green triangle), 3mm (blue square) and 4mm (red dot) of laser shock diameter and (b) evolution of blister height with the size of debonded area (same marker code)

From such important demonstration, it is proposed to combine both LASAT experiments and buckling analysis with interrupted thermal cycles on an other sample submitted to the same experimental procedure shown in Fig. 4. In this case, the complete spallation occurred at 400 cycles and a series of laser shock was achieved after every 50 cycles. As previously established for a similar plate sample, the adhesion level measured by LASAT was decreasing with the number of cycles. From this experiment, one buckle profile was thoroughly analyzed after a laser shock achieved at 50 cycles. The profile of this buckled area was then analyzed every 50 cycles. The evolution of the buckle profile from 50 to 350 cycles (before final spallation at 400 cycles) is shown in Figure 7. Firtsly, no macroscopic failure of the ceramic has been observed after 350 cycles. The maximum amplitude of the buckle was 265 $\mu$m for a radius of about 4.1 mm. Secondly, from 50 to 300 cycles, almost no drastic growth of the interfacial decohesion has been observed, whilst the blister has increased progressively from 10 to 125 $\mu$m approximatively. Moreover, the top-view observations of the 3D-profil show a quasi-perfect circularity of the blister, see insert in Figure 7. Consequently, the assessment of the delamination induced by thermal cycling on a pre-cracked blister can be evaluated consistently through the measurements of the diameter of the debonded area together with the blister height, Figure 8.

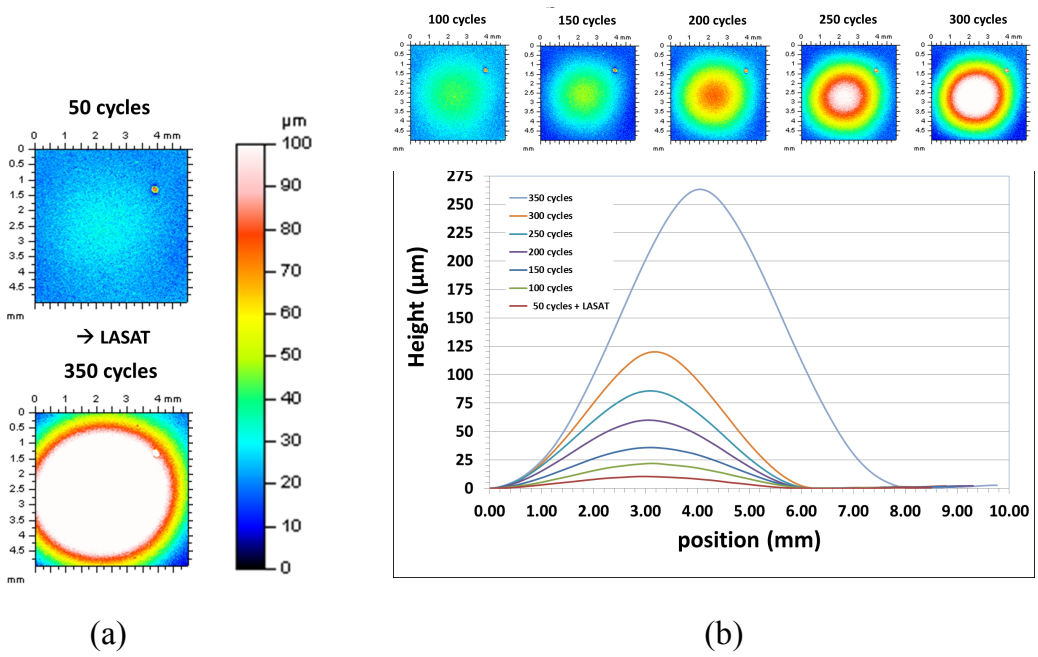



Figure 7: Evolution of blister profile with thermal cycling, initial debonding has been introduced by LASAT after 50 cycles (a) Detail of 3D profilometer measurement at 50 cycles and after 350 cycles (b) Evolution with number of cycles of one profile; inserts amplitude corresponds to (a)

Further thermal cycling has led to a two steps evolution of the chosen blister as compared to its initial configuration. Firstly, the radius of the debonded area, R, was evolving slightly meanwhile the height of the blister, $\delta$, was increasing drastically with the number of cycles for N $\leq$300, Figure 7 and 8. Secondly, a jump in the size of the debonded area was observed for N $>$ 300. The first step could be assumed to correspond to a constant location of the crack tip, for 100 $\leq$N $\leq$300. For N$>$300, interfacial crack has grown. These observations yield two main points. It is obvious that the debonding obtained by laser shock is associated to local stress relaxation. However, after debonding, the continuous blistering of the ceramic layer shows that thermal cycling is still inducing a certain amount of mechanical loading. If one assumes that after a given number of cycles (here around 300) interfacial debonding occurs, it does mean that the critical interfacial toughness has been reached at this point. The mechanism of blistering does not need to be identified to validate the above assumptions.

### *4.2. Evaluation of interfacial toughness for a single blister*

The above observations could be used in a linear elastic fracture mechanics (LEFM) approach that yields the following assumptions:

- i) For 100 $\leq$N $\leq$300, $G < G_c(N)$ ;
- ii) For N $>$ 300, $G = G_c(N)$

where $G$ indicates the energy release rate, and $G_c$ indicates its critical value, the so-called interfacial toughness that is assumed to decrease with N [27, 28]. To evaluate $G_c$, it is thus needed to determine carefully $G$ for the number of cycles for which further interfacial crack propagation has been observed. We propose to develop firstly analytic evaluation of $G$ based on assumption proposed by Hutchinson and coworkers [29, 30]. Secondly, we will derive $G$ from the measurement of local buckling of the blister.

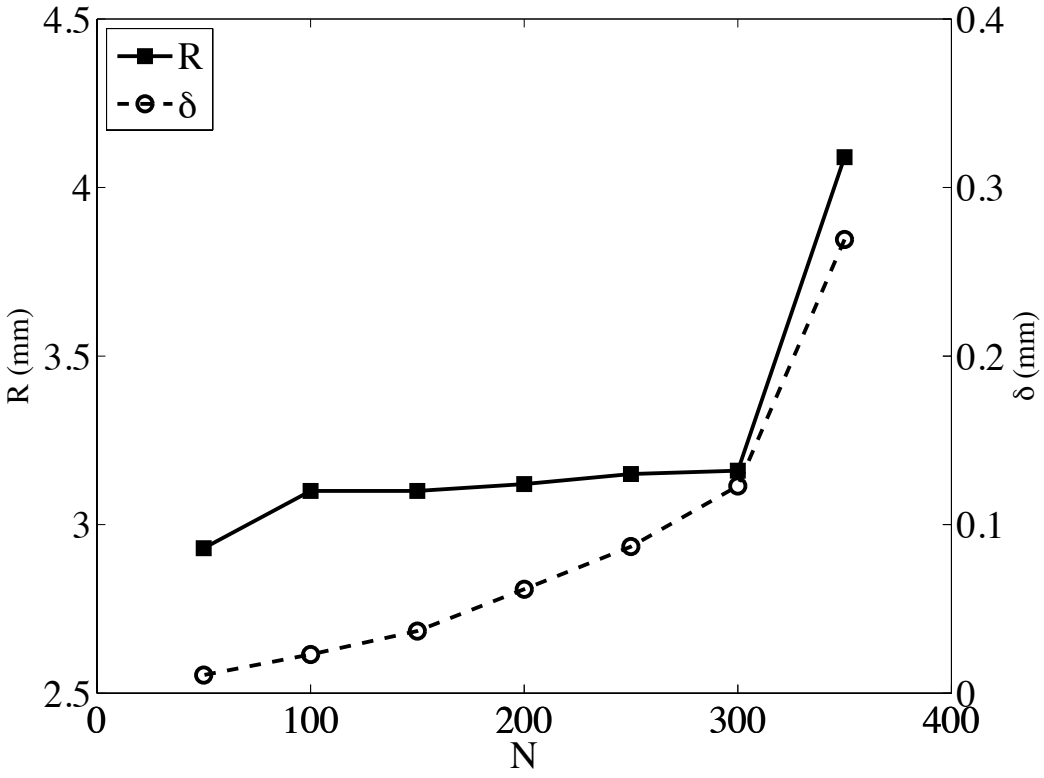



Figure 8: Geometrical evolution of one blister under thermal cycling; an initial delamination has been introduced after 50 cycles, the measurements are the radius R of the blister and its height $\delta$

*4.2.1. Interfacial toughness based on clamped blister analysis*

The assessment of elastic energy in a blister for a ceramic layer deposited on a metallic substrate has been widely commented by Hutchinson and coworkers [29, 31, 32, 30]. For a circular blister, similar to the obtained blister after laser shock, the authors have mainly proposed to focus on perfectly clamped blister on its edge loaded by in-plane equibiaxial residual stress state, where the magnitude of residual stresses is $\sigma_0$. The residual stresses can be obtained for thin films from the measurement of beginning of blistering [30]. This work is in continuity with previous works proposed by Hutchinson and coworkers cited above using these assumptions to deal with TBC considered as homogeneous media, that is to say ignoring the impact of micro defects within columnar microstructure of EB-PVD TC. In our case, experimental blister measurements yields evolution of stress according to equation 1:

$$\sigma_0 = \sigma_c \left[ c_1 \left( \frac{\delta}{h} \right)^2 + 1 \right] \tag{1}$$

$\delta$ being the maximum height of the blister, $h$ the thickness of the ceramic layer, $c_1$ being a function of the Poisson coefficient of the ceramic layer $\nu$, eq. 3:

$$c_1 = 0.2473(1+\nu) + 0.231(1-\nu^2) \tag{2}$$

and where critical stress at buckling $\sigma_c$ is derived from elastic assumption, eq. 3:

$$\sigma_c = 1.2235 \frac{E}{1-\nu^2} \left( \frac{h}{R} \right)^2 \tag{3}$$

E corresponding to the Young modulus of the ceramic layer and R being the radius of the delaminated area. This assumption, leads to the set of equations (4) and (5):

$$\frac{G}{G_0} = c_2\left[1 - \left(\frac{\sigma_c}{\sigma_0}\right)^2\right] \tag{4}$$

$$G_0 = (1-\nu)h_1\sigma_0^2/E \tag{5}$$

where $c_2$ is a function of the Poisson coefficient of the ceramic layer $\nu$: $c_2 = [1 + 0.9021(1-\nu)]^{-1}$.

Under the assumptions of buckled-driven delamination, $G_0$ corresponds to the stored energy in the system within an equibiaxial residual stress level $\sigma_0$. The evolution of energy release rate $G$ could be derived from the global geometrical evolution of the blister and has been plotted as a function of N from experimental measurement obtained for E=50 GPa, $\nu$=0.1 and $h_1$=180 $\mu$m, Figure 9. This result is fully consistent with an increase of $G$ without delamination and finally leading to delamination for $G = G_c$. At delamination, in our case for N=300 cycles, $G$ tends to 36 J/m$^2$. The systematic error induced by radius measurement is about $\pm$50 $\mu$m. This error induces a maximum of $\pm$7% on $G$ evaluation, and has been added to the Figure 9 using error bar. It is worth noting that $G$ is continuously increasing with N, even after increase in delamination. This raises questions of the validity of chosen assumptions, mainly the perfect clamped boundary condition.

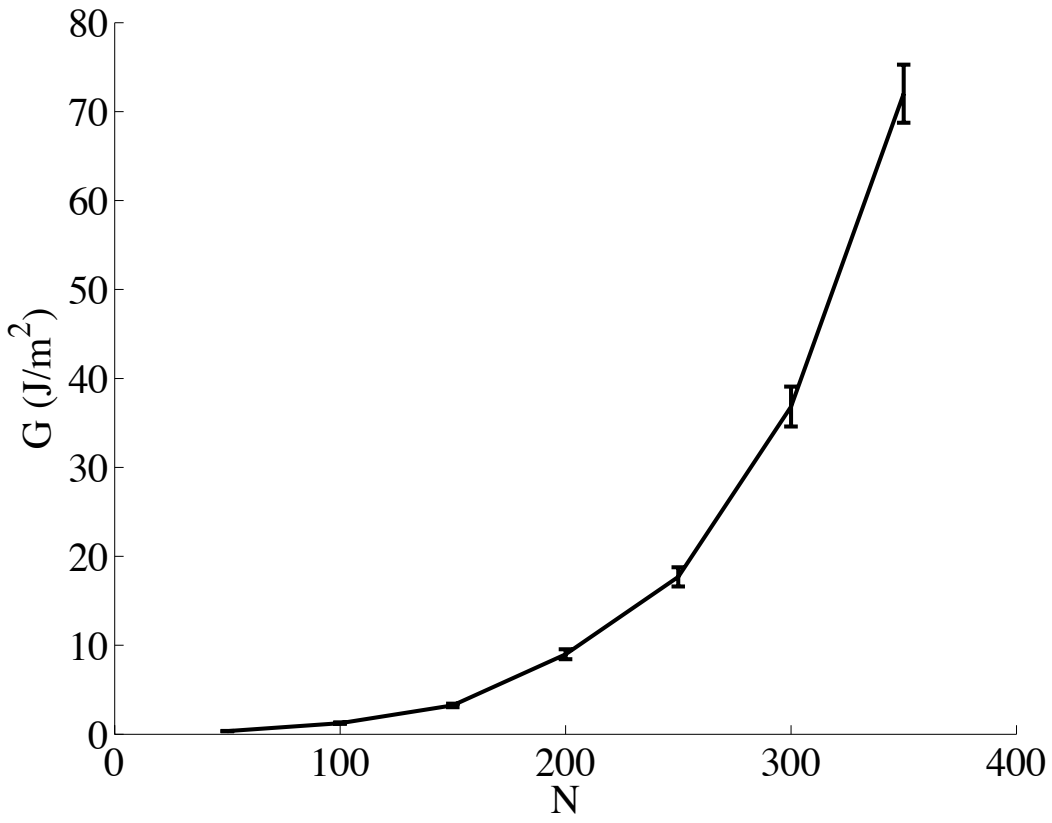



Figure 9: Evolution of energy release rate G as a function of the number of thermal cycles N assuming a blister perfectly clamped on its edge

*4.2.2. Interfacial toughness based on local analysis of crack tip opening*

To reach more accurate values of local loading, pseudo stress intensity factors can be used. These pseudo-SIFs are derived from interfacial displacement [33, 34]. Together with global blister measurements, the precision of 3D profilometer has enabled to measure locally the out-of-plane position of the blister in the vicinity of the crack tip, figure 10, corresponding to the vertical surface displacement of the coating after the laser shock and after thermal cycling.

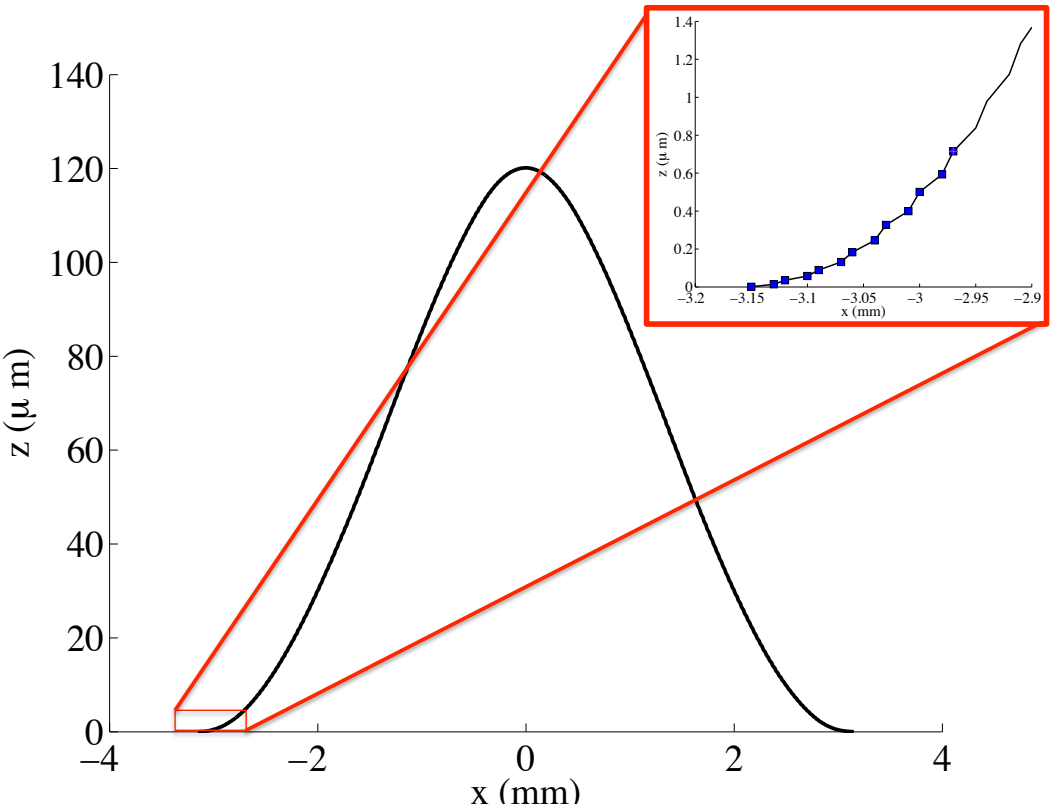



Figure 10: Out-of-plane positions obtained from 3D measurement of the blister for N=300 cycles from Figure 7; insert is magnification of the curve where $\delta_y^i$ is measured see text for details

A simple assumption consists in associating crack tip opening to the out-of-plane position measurements of the coating surface, $\delta_y^i$. That is to say that one assumes to neglect the deformation of the coating itself along its thickness, after laser shock and thermal cycling. Moreover, because there is no measurement of the in-plane displacement, one also neglects the associated terms. Thus pseudo-SIF can be evaluated as proposed for instance by Nagashima et al. (see [33] for complete equations), set of equations 6 to 8:

$$K_1^i = C[\delta_y^i(\cos Q + 2\varepsilon \sin Q)]/\sqrt{r_i/(2\pi)} \tag{6}$$

$$K_2^i = C[-\delta_y^i(\sin Q - 2\varepsilon \cos Q)]/\sqrt{r_i/(2\pi)} \tag{7}$$

$$G = \beta(K_1^2 + K_2^2) = \beta C^2(1 + 4\varepsilon^2) \lim_{r\to 0}[\delta_y^2]/(r/2\pi)) \tag{8}$$

where $C$ is a material parameters function of Dundur's parameters $\varepsilon$ and $\beta$, $Q$ being function of the current point, defined by it distance to the crack tip $r$, considering a crack length $a$. These quantities are defined

as:

$$\varepsilon = \frac{1}{2\pi}\left(\frac{\frac{\kappa_1}{\mu_1}+\frac{1}{\mu_2}}{\frac{\kappa_2}{\mu_2}+\frac{1}{\mu_1}}\right) \tag{9}$$

$$\beta = \frac{(\kappa_1+1)/\mu_1 + (\kappa_2+1)/\mu_2}{16\cosh^2(\varepsilon\pi)} \tag{10}$$

$$C = \frac{2\cosh(\varepsilon\pi)}{(\kappa_1+1)/\mu_1 + (\kappa_2+1)/\mu_2} \tag{11}$$

$$Q = \varepsilon \ln(r/2a) \tag{12}$$

where layers elasticity is defined by:

$$\mu_i = \frac{E_i}{2(1+\nu_i)}\,(i=1,2) \tag{13}$$

$$\kappa_i = 3-4\nu_i\,(i=1,2) \tag{14}$$

assuming plane strain condition.

The set of equations 6 to 8 takes into consideration both geometry of the crack tip, $\delta_y$ being the out-of-plane opening displacement between crack lips, and elasticity mismatch between layers $\varepsilon$ derived from Dundur's parameters, eq. 9 to 11. Here subscript 1 and 2 are associated to the coating and the substrate respectively.

Because blister measurements are limited to the resolution of the acquisition, pseudo-SIF can only be evaluated through discrete analysis similar to the one used for finite element analysis.

$$K_1 = \frac{r_a K_1^b - r_b K_1^a}{r_a - r_b} \tag{15}$$

$$K_2 = \frac{r_a K_2^b - r_b K_2^a}{r_a - r_b} \tag{16}$$

To apply this method, it should be carefully defined what are the optimum location of test points, namely points $a$ and $b$, eq. 15 and 16. For finite element analysis, it is straightforward to use points as close as possible to the crack tip, since exact value should be found for point at the very crack tip [33]. However, from experimental measurement, it is difficult to obtain precisely the crack tip location and moreover, to obtain accurate value of out-of-plane displacement for points too close to the crack tip. Thus we choose to firstly determine the location of the crack tip by defining the point $a$ as the first point reaching the minimum vertical value. In the present study $G$ should reach its maximum value at the beginning of further interfacial crack delamination, for N=300. For higher number of thermal cycles, it has been evidenced that $G_c$ could be only constant or decreasing with aging [27, 28, 35]. Then, we perform a sensitivity analysis on the location of the second point $b$ so as to obtain decrease or constant $G$ values for N$\geq$300. This sensitivity analysis has shown that for $r_b$-$r_a$>100 $\mu$m, $G$ was increasing monotonously and that for $r_b$-$r_a$<60 $\mu$m, maximum $G$ values was decreasing. Thus $r_b$-$r_a$ =100 $\mu$m was seen as an optimum value both respecting the consistency of $G$ evolution and being large enough as compared to spatial resolution of the chosen method. This chosen value should be seen as a non-local parameter classically used in local approach of fracture (e.g. see [36]).

The elastic behavior is here considered for a ceramic layer made of columnar YSZ and an alumina oxide layer. This point is motivated by the observed localization of crack between the ceramic and the TGO. Finally, the evolution of energy release rate $G$ derived from the local geometrical evolution of the blister has been plotted as a function of N from experimental measurement obtained for $E_1$=50 GPa and $\nu_1$=0.1, $E_2$=400 GPa and $\nu_2$=0.23, for YSZ EB-PVD and pure alumina respectively [37, 38, 39]. The value of $r_b$-$r_a$ was set to 100 $\mu$m and $r_a$ was determined carefully for each measurement.

This method has enabled to obtain again a clear increase of $G$ up to delamination, then a decrease of

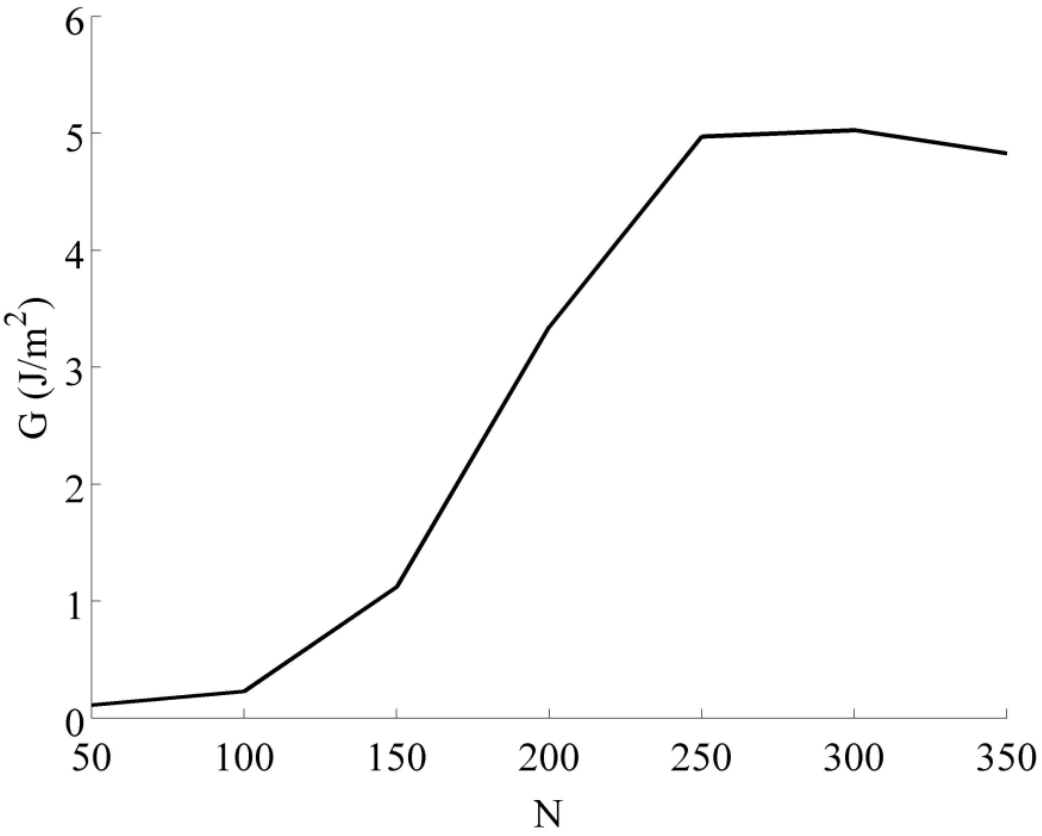



Figure 11: Evolution of energy release rate G as a function of the number of thermal cycles N ; G is derived from pseudo SIF values associated to local measurement of blistering in the vicinity of the crack tip

$G$ after delamination was reached. It is worth noting that this method yields much more lower value of $G_c$ as compared to $G$ derived from perfectly clamped blister assumption. This point will be discussed in the sequel. At last but not least, the chosen location of the crack tip is the minimum possible value for $r_a$. Thus, if delaminated area is higher than assumed, the derived $G$ values would be lower than the one found with chosen $r_a$ value. Thus, the proposed evolution of $G$ finally consists in an upper bound evaluation of $G$ with the chosen method.

## 5. Discussion

Through this study, it has been established that the LASAT method was sensitive to both processing condition and aging. The reference roughness process condition has appeared to drive to the lowest number of thermal cycles leading to TC spallation, whereas initial smooth interface in the tested conditions has led to no TC failure. Cross-section observations, achieved at a limited number of cycles, have shown that local decohesion was observed associated to local roughness amplified by the rumpling phenomenon. Thus, the quality of the smooth polishing could be associated to a limitation of rumpling for the tested processing conditions. Moreover, LASAT-2D curves are fully consistent with this point since smooth polishing yields a lower decohesion than other processing conditions for a same laser power density. Surprisingly, high grit blasting condition has exhibited a larger number of defects after 200 thermal cycles but yields to better resistance to final TC spallation as compared to reference processing condition. Similar analysis, using the initial roughness as a process parameter have exhibited different ranking: for Chirivi et al, no clear influence

of surface preparation was observed for (Ni,Pt)Al coating CMSX4 superalloy [40], whereas for Meier and coworkers, heavy grit blasting led to shortest life as compared to light grit blasting and hand polished [41, 42, 2]. On the other hand, Vaidyanathan et al have shown that optimal life was associated to local ridges, and therefore initial roughness that directly impacts local stresses promoting debonding from defects [43, 44, 45]. Therefore the observed influence of initial surface preparation in the present study should be deeper analyzed by increasing the number of tested conditions and subsequent reliability of sampling. However, the ranking of different process conditions obtained by LASAT is fully consistent with the fatigue life to spallation under thermal cycling.

Aging in EB-PVD TBCs has been widely documented [46, 42, 4, 7]. One of the major results about damage mechanisms is that the interfacial degradation precedes final spallation of the ceramic layer. Moreover, it has been clearly established that the locus of damage varies as a function of applied thermal loading: for isothermal condition the damage is localized at the metal (bond-coat) / thermal grown oxide interface whereas for thermal cycling the damage is a localized at the thermal grown oxide / YSZ (top-coat) interface. Using laser shock, the decohesion mechanism induced by shock wave is definitively different from the damage mechanism induced by thermal loading. However, the decohesion induced by laser shock after thermal cycling (here for N>10 cycles) is localized at the thermal grown oxide / YSZ (top-coat) interface. This consistency helps to gain confidence in the damage evolution deduced from laser shock experiment.

One of the major interests of laser shock for interfacial toughness characterization consists in the knowledge of the localization of defect. Thus evaluation of defect evolution gains in precision for both delamination and buckling measurements. This methodology has been applied previously to determine interfacial behavior under mechanical loading [14]: a defect was introduced by laser shock in a specimen and mechanical loading was applied in a second step. The obtain damage evolution was very similar to the current observation made in the current paper. During mechanical loading, it was observed firstly increase of the blister height (increase in buckling) without further delamination from the initial defect. Secondly, further interfacial crack propagation was observed by in situ analysis. This similarity between mechanical loading and thermal cycling, in buckling and delamination mechanisms helps to gain confidence in the evaluation of interfacial toughness. Besides, its has been shown in the present study that the blistering was not affected by LASAT conditions. Thus, because under thermal cycling, nothing but aging of the microstructure takes place, the observed evolution of blister induced by LASAT should be only the consequence of thermal cycling, induced thermo-mechanical fatigue (mainly CTE mismatch between layers together with oxide strain growth) and this microstructure aging, without artifact induced by LASAT. Thus, this point opens new ways to address progressive damage assessment on EB-PVD coatings under thermal cycling.

Based on proposed analysis, we observed that the range of interfacial toughness is large: after 300 thermal cycles, the obtained $G_c$ varies between 5 to 36 J/m$^2$ depending on the chosen method of evaluation. However, in the open literature, most of results are limited to as-processed condition for various loading, from pure mode I to pure mode II [47, 27, 28, 48] and for APS TC and/or MCrAlY coating after aging, see Table 2. Thus, because no unified method is used benchmarking both the testing method of adhesion and the analysis yielding interfacial toughness is needed in the community. Nevertheless, the obtained values in this study could be compared to combined results proposed in the literature: for Vaunois et al, after 250 thermal cycles at 1100 °C for 1h dwell, initial toughness decreases by a factor 3, for Thery et al, using a similar system, initial toughness is about 110 J/m$^2$, leading to 36 J/m$^2$ after 250 thermal cycles at 1100 °C which value is fully consistent with our findings derived from Hutchinson approximation. But, the large scatter observed in the study of Vaunois limits this conclusion. For Bahr et al, isothermal aging at 1100 °C decreases the interfacial toughness from more than 81 to 37 J/m$^2$, even though the nature of the BC and the thickness of the TC (250 $\mu m$) were different from the present study [49].

One of the main advantages of the proposed methodology using LASAT consists in its low complexity as compared to more standard set-up (4-point bending, tensile adhesion test...) where the gluing of a counterplate is challenging for the test success, artifacts the loading and is source of scatter. Besides, the obtained stress state condition with blister induced by LASAT is multiaxial and thus mimics accurately the stress state induced by either processing or thermal cycling.

The evaluation of $G$ and $G_c$ from experimental measurement using pseudo-SIF appears as a promising tool for further investigation. Even though the proposed measurement of $G_c$ is limited to only one point of

Table 2: toughness evaluation for different testing and analysis methodology

| TC | BC | Method | Analysis | Mixity angle ( °) | Aging | Gc (J/m$^2$) | Ref. |
|---|---|---|---|---|---|---|---|
| APS | NiCoCrAlY | compression | FEA | -56 | no | 110-130 | [50] |
| EB-PVD | CoNiCrAlY | push-out/shear | analytical | -90 | isothermal | 120 (hox=2 $\mu$m) | [35] |
| | | | | | | 20 (hox=4.5 $\mu$m) | |
| EB-PVD | NiCoCrAlY | bending | FEA | 20 | no | 57±21 | [48] |
| EB-PVD | NiCoCrAlY | 4-point bending | analytical | 20 | no | >81 | [49] |
| | | | | 20 | 1000 °C 100 h | 63 | [49] |
| | | | | 20 | 1100 °C 10 h | 37 | [49] |
| EB-PVD | (Ni,Pt)Al | 4-point bending | analytical | 20 | no | 110 | [27] |
| EB-PVD | (Ni,Pt)Al | | FEA | 20 and 70 | FCT 250 cycles | | |
| | | | | | 1100 °C 1h | G0/3±3G0 | [28] |

aging, where debonding directly induced by thermal cycling is observed, it is possible to use this methodology under mechanical loading for any aging. FEA could be helpful to validate the chosen assumption that clearly has led to a minor bound of $G_c$ as compared to clamped blister assumption.

Thus it has also been shown that classical assumptions used for interfacial toughness evaluation could be revisited thanks to a better evaluation of the crack tip morphology (in-plane localization) and crack geometry (opening) using laser shock. A new question emerges from these observations: the process zone, the zone of transition from damaged and "sane" interface, should be accurately determined to finally obtain a precise evaluation of interfacial toughness. This kind of work have been recently achieved by using both focused ion beam coupled with scanning electron microscopy (FIB-SEM) 3D serial sectioning tomography and LASAT to determine easily the locus of a crack tip [11]. The measured process zone size is of about 20 $\mu$m which is below the systematic error made in the present study for the localization of the crack tip position that was of about ±50 $\mu$m. However, this error is close to the process zone size. Subsequently, the uncertainty in crack measurement used in the present study seems to be relevant and should be integrated in the evaluation of mechanical properties in future studies.

## Conclusions

This study has investigated several aspects of LASAT associated to thermal cycling. This method appeared to be very fruitful to gain both knowledge in damage mechanisms and direct evaluation of properties of a typical EB-PVD TBC system under thermal cycling aging. It has been shown that LASAT-2D curves could be used to establish a ranking between different coating processing. The direct comparison to life determined by TC spallation is consistent with this obtained ranking for typical thermal cycling achieved under lab-air oxidation. It has also been established that with significant thermal cycling but kept to less than 10% of the life of the specimen, the locus of damage induced by LASAT is the TC/TGO interface. Thus the LASAT investigation is consistent with observed localization of damage for thermal cycling. As a major result of this study, it has been established that the debonded area induced by a given laser power density increases monotonically with the number of cycles. The use of LASAT has also been evidenced not to artifact damage mechanisms known for TBC under thermal cycling: the laser shock diameter does not impact the TC blistering, validating that LASAT only damages the TC/TGO interface of aged EB-PVD TBC. Because the use of LASAT enables to precisely determine the location and size of an initial interfacial defect, the full measurement of blistering during thermal cycling has led to new possibilities of interfacial toughness evaluation.

## Acknowledgements

The authors are grateful to Safran Aircraft Engines to have provided samples and partially funded this study. Authors are very grateful to Pascal Bilhe, Andre Malie and Jean-Yves Guedou for their investment in this partnership.

## References

[1] David R Clarke, Matthias Oechsner, and Nitin P Padture. Thermal-barrier coatings for more efficient gas-turbine engines. *MRS bulletin*, 37(10):891–898, 2012.

[2] NM Yanar, M Helminiak, GH Meier, and FS Pettit. Comparison of the failures during cyclic oxidation of yttria-stabilized (7 to 8 weight percent) zirconia thermal barrier coatings fabricated via electron beam physical vapor deposition and air plasma spray. *Metallurgical and Materials Transactions A*, 42(4):905–921, 2011.

[3] Marion Bartsch, Bernd Baufeld, S. Dalkiliç, L. Chernova, and Michael Heinzelmann. Fatigue cracks in a thermal barrier coating system on a superalloy in multiaxial thermomechanical testing. *International Journal of Fatigue,*, 30(2):211–218, 2 2008.

[4] C. Courcier, V. Maurel, L. Remy, S. Quilici, I. Rouzou, and A. Phelippeau. Interfacial damage based life model for eb-pvd thermal barrier coating. *Surface and Coatings Technology*, 205(13-14):3763 – 3773, 2011.

[5] V.K. Tolpygo, D.R. Clarke, and K.S. Murphy. Oxidation-induced failure of EB-PVD thermal barrier coatings. *Surf. Coat. Technol.*, 146-147:124–131, 2001.

[6] Bauke Heeg, Vladimir K Tolpygo, and David R Clarke. Damage evolution in thermal barrier coatings with thermal cycling. *Journal of the American Ceramic Society*, 94:s112–s119, 2011.

[7] R. Soulignac, V. Maurel, L. Remy, and A. Koster. Cohesive zone modelling of thermal barrier coatings interfacial properties based on three-dimensional observations and mechanical testing. *Surf. Coat. Technol.*, 237(0):95 – 104, 2013.

[8] Albert Manero II, Alex Selimov, Quentin Fouliard, Kevin Knipe, Janine Wischek, Carla Meid, Anette M Karlsson, Marion Bartsch, and Seetha Raghavan. Piezospectroscopic evaluation and damage identification for thermal barrier coatings subjected to simulated engine environments. *Surface and Coatings Technology*, 323:30–38, 2017.

[9] V. Maurel, R. Soulignac, L. Helfen, T.F. Morgeneyer, A. Koster, and L. Remy. Three-dimensional damage evolution measurement in ebpvd tbc using synchrotron laminography. *Oxidat. of Metals*, 79(3-4, SI):313–323, 2013.

[10] D Khoshkhou, M Mostafavi, C Reinhard, MP Taylor, DS Rickerby, IM Edmonds, HE Evans, TJ Marrow, and BJ Connolly. Three-dimensional displacement mapping of diffused pt thermal barrier coatings via synchrotron x-ray computed tomography and digital volume correlation. *Scripta Materialia*, 115:100–103, 2016.

[11] Anne Dennstedt, Fabrice Gaslain, Marion Bartsch, Vincent Guipont, and Vincent Maurel. Three-dimensional characterization of cracks in a columnar thermal barrier coating system for gas turbine applications. *Integrating Materials and Manufacturing Innovation*, pages 1–13, 2019.

[12] Vincent Guipont, Michel Jeandin, Sebastien Bansard, Khiam Aik Khor, Mariette Nivard, Laurent Berthe, Jean-Paul Cuq-Lelandais, and Michel Boustie. Bond strength determination of hydroxyapatite coatings on ti-6al-4v substrates using the laser shock adhesion test (lasat). *Journal of Biomedical Materials Research Part A*, 95(4):1096–1104, 2010.

[13] Geoffrey Bégué, Grégory Fabre, Vincent Guipont, Michel Jeandin, P Bilhe, Jean Yves Guedou, and François Lepoutre. Laser shock adhesion test (lasat) of eb-pvd tbcs: Towards an industrial application. *Surface and Coatings Technology*, 237:305–312, 2013.

[14] Hélène Sapardanis, Vincent Maurel, Alain Köster, Steve Duvinage, François Borit, and Vincent Guipont. Influence of macroscopic shear loading on the growth of an interfacial crack initiated from a ceramic blister processed by laser shock. *Surface and Coatings Technology*, 291:430–443, 2016.

[15] Mario Schweda, Tilmann Beck, Marita Offermann, and Lorenz Singheiser. Thermographic analysis and modelling of the delamination crack growth in a thermal barrier coating on Fecralloy substrate. *Surface and Coatings Technology*, 217:124–128, February 2013.

[16] Hélène Sapardanis, Vincent Guipont, François Borit, Antoine Debray, Alain Köster, and Vincent Maurel. Study of the interface strength and residual stresses within plasma sprayed alumina coatings involving lasat (laser shock adhesion test). In *International thermal spray conference 2017*, pages 315–321. DVS Berichte, 2017.

[17] V Gupta, AS Argon, JA Cornie, and DM Parks. Measurement of interface strength by laser-pulse-induced spallation. *Materials Science and Engineering: A*, 126(1-2):105–117, 1990.

[18] R Ikeda, H Cho, A Sawabe, and M Takemoto. Laser spallation method to measure strength against mode-i decohesion of cvd diamond films. *Diamond and related materials*, 14(3-7):631–636, 2005.

[19] Hitoshi Akamatsu, Manabu Satou, Takashi Sato, Amit Jain, Vijay Gupta, and Akira Hasegawa. Evaluation of bonding strength between yttria coating and vanadium alloys for development of self-cooled blanket. *Journal of Nuclear Materials*, 417(1-3):1253–1256, 2011.

[20] Akira Kobayashi, Amit Jain, Vijay Gupta, and V Kireev. Study on the interface strength of zirconia coatings by a laser spallation technique. *Vacuum*, 73(3-4):533–539, 2004.

[21] M Arrigoni, Sophie Barradas, M Braccini, M Dupeux, Michel Jeandin, M Boustie, C Bolis, and L Berthe. A comparative study of three adhesion tests (en 582, similar to astm c633, lasat (laser adhesion test), and bulge and blister test) performed on plasma sprayed copper deposited on aluminium 2017 substrates. *Journal of adhesion science and technology*, 20(5):471–487, 2006.

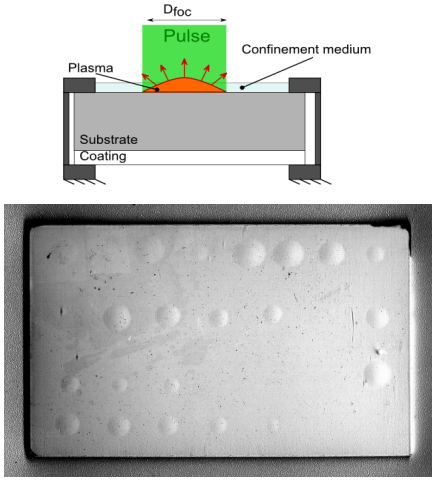
[22] L. Berthe, M. Arrigoni, M. Boustie, J. P. Cuq-Lelandais, C. Broussillou, G. Fabre, M. Jeandin, V. Guipont, and M. Nivard. State-of-the-art laser adhesion test (LASAT). *Nondestructive Testing and Evaluation*, 26(3-4, SI):303–317, 2011.
[23] Vincent Guipont, Vincent Maurel, Marion Bartsch, and Anne Dennstedt. Interfacial toughness evolution under thermal cycling by laser shock and mechanical testing of an eb-pvd coating system. TBC V, Irsee Germany, ECI, 2018.
[24] M Boustie, J P Cuq-Lelandais, C Bolis, L Berthe, S Barradas, M Arrigoni, T de Resseguier, and M Jeandin. Study of damage phenomena induced by edge effects into materials under laser driven shocks. *Journal of Physics D: Applied Physics*, 40(22):7103–7108, November 2007.
[25] Vladimir A. Esin and Fabrice Gaslain. Experimental and thermodynamic analysis of differences in phase transformation of pt-modified nickel aluminide coating during isothermal and cyclic oxidation. *Surface and Coatings Technology*, 307:915 – 925, 2016.
[26] G. Fabre. *Influence des propriétés optiques et de l'endommagement de barrières thermiques EB-PVD pour la mesure d'adhérence par choc laser LASAT-2D (in French)*. PhD thesis, Mines ParisTech, 2013.
[27] P. Y. Thery, M. Poulain, M. Dupeux, and M. Braccini. Spallation of two thermal barrier coating systems: experimental study of adhesion and energetic approach to lifetime during cyclic oxidation. *Journal of Materials Science*, 44(7):1726–1733, 2009.
[28] Jean-Roch Vaunois, Martine Poulain, Pascale KanoutÃl', and Jean-Louis Chaboche. Development of bending tests for near shear mode interfacial toughness measurement of eb-pvd thermal barrier coatings. *Engineering Fracture Mechanics*, 171:110 – 134, 2017.
[29] J.W. Hutchinson, M.D. Thouless, and E.G. Liniger. Growth and configurational stability of circular, buckling-driven film delaminations. *Acta Metallurgica et Materialia*, 40(2):295 – 308, 1992.
[30] Joel P. McDonald, M.D. Thouless, and Steven M. Yalisove. Mechanics analysis of femtosecond laser-induced blisters produced in thermally grown oxide on si(100). *Journal of Materials Research*, 25(6):1087?1095, 2010.
[31] M.D. Thouless, J.W. Hutchinson, and E.G. Liniger. Plane-strain, buckling-driven delamination of thin films: Model experiments and mode-ii fracture. *Acta Metallurgica et Materialia*, 40(10):2639 – 2649, 1992.
[32] Matthew R. Begley and Joseph M. Ambrico. Delamination of thin films from two-dimensional interface flaws at corners and edges. *International Journal of Fracture*, 112(3):205–222, Dec 2001.
[33] Toshio Nagashima, Youhei Omoto, and Shuichi Tani. Stress intensity factor analysis of interface cracks using x-fem. *International Journal for Numerical Methods in Engineering*, 56(8):1151–1173.
[34] J.W. Hutchinson and Z. Suo. Mixed mode cracking in layered materials. volume 29 of *Advances in Applied Mechanics*, pages 63 – 191. Elsevier, 1991.
[35] Sang-Seok Kim, Yu-Fu Liu, and Yutaka Kagawa. Evaluation of interfacial mechanical properties under shear loading in eb-pvd tbcs by the pushout method. *Acta Materialia*, 55(11):3771 – 3781, 2007.
[36] Zdenek P Bazant. Nonlocal damage theory based on micromechanics of crack interactions. *Journal of engineering mechanics*, 120(3):593–617, 1994.
[37] M. Fukuhara and I. Yamauchi. Temperature-dependence of the elastic-moduli, dilational and shear internal frictions and acoustic-wave velocity for alumina, (y)tzp and beta-(sial) on ceramics. *Journal Materials Sciences*, 28:4681–4688, 1993.
[38] J. Frachon. *Multiscale approach to predict the lifetime of EB-PVD thermal barrier coatings*. PhD thesis, Mines ParisTech, 14 Decembre 2009.
[39] V. Maurel, E.P. Busso, J. Frachon, J. Besson, and F. N'Guyen. A methodology to model the complex morphology of rough interfaces. *International Journal of Solids and Structures*, 51(19):3293 – 3302, 2014.
[40] L Chirivi and JR Nicholls. Influence of surface finish on the cyclic oxidation lifetime of an eb-pvd tbc, deposited on ptal and pt-diffused bondcoats. *Oxidation of metals*, 81(1-2):17–31, 2014.
[41] A. G. Evans, D. R. Mumm, J. W. Hutchinson, G. H. Meier, and F. S. Pettit. Mechanisms controlling the durability of thermal barrier coatings. *Progress in Materials Science*, 46(5):505 – 553, 2001.
[42] N. Yanar, F. Pettit, and G. Meier. Failure characteristics during cyclic oxidation of yttria stabilized zirconia thermal barrier coatings deposited via electron beam physical vapor deposition on platinum aluminide and on nicocraly bond coats with processing modifications for improved performances. *Metallurgical and Materials Transactions A*, 37(5):1563–1580, 2006.
[43] Krishnakumar Vaidyanathan, Eric H. Jordan, and Maurice Gell. *Acta Materialia*, 52(5):1107 – 1115, 2004.
[44] D. R. Mumm, A. G. Evans, and I. T. Spitsberg. Characterization of a cyclic displacement instability for a thermally grown oxide in a thermal barrier system. *Acta Materialia*, 49(12):2329 – 2340, 2001.
[45] V. Maurel, L. Remy, M. Harvey, H. Tezenas du Montcel, and A. Koster. The respective roles of thermally grown oxide roughness and NiAl coating anisotropy in oxide spallation. *Surface and Coatings Technology*, 215:52 – 61, 2013.
[46] I.T. Spitsberg, D.R. Mumm, and A.G. Evans. On the failure mechanisms of thermal barrier coatings with diffusion aluminide bond coatings. *Materials Science and Engineering A*, 394(1-2):176 – 191, 2005.
[47] SQ Guo, DR Mumm, Anette M Karlsson, and Y Kagawa. Measurement of interfacial shear mechanical properties in thermal barrier coating systems by a barb pullout method. *Scripta Materialia*, 53(9):1043–1048, 2005.
[48] Christoph Eberl, Xi Wang, Daniel S. Gianola, Thao D. Nguyen, Ming Y. He, Anthony G. Evans, and Kevin J. Hemker. In situ measurement of the toughness of the interface between a thermal barrier coating and a ni alloy. *Journal of the American Ceramic Society*, 94(s1):s120–s127, 2011.
[49] H-A Bahr, H Balke, T Fett, I Hofinger, G Kirchhoff, D Munz, A Neubrand, AS Semenov, H-J Weiss, and YY Yang. Cracks in functionally graded materials. *Materials Science and Engineering: A*, 362(1-2):2–16, 2003.
[50] W. Zhu, L. Yang, J.W. Guo, Y.C. Zhou, and C. Lu. Determination of interfacial adhesion energies of thermal barrier coatings by compression test combined with a cohesive zone finite element model. *International Journal of Plasticity*, 64:76 – 87, 2015.

**Additional material**

# LASAT and THERMAL CYCLING of TBC

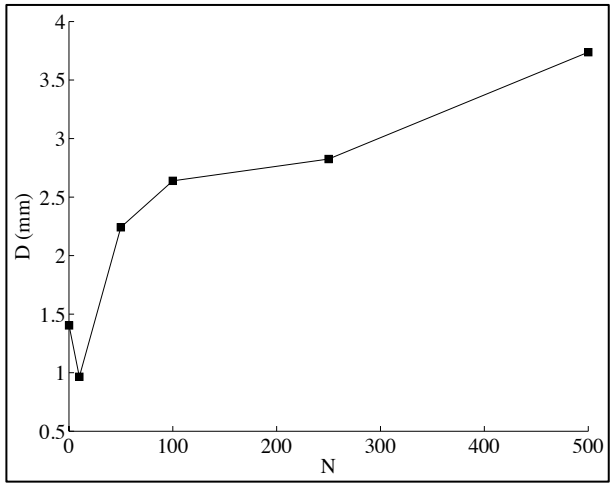
## BLISTERING

Series of laser shocks at different number of cycles



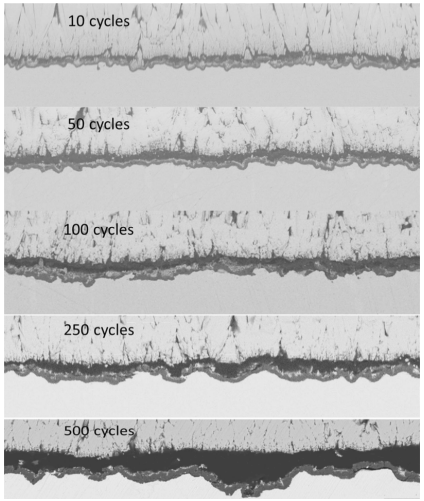

## DELAMINATION

Same laser shock at different number of cycles




## INTERFACE

Interfacial damage at different number of cycles




- **Crack diameter evolution is consistent with a significant decrease of the interfacial toughness with thermal cycling**
- **After 10 cycles, the weakest interface revealed both by LASAT and thermal cycling is the TGO/TC interface**